IMAGE PROCESSING IN 3-D STANDING-WAVE FLUORESCENCE MICROSCOPY

Vijay Krishnamurthi*, Brent Bailey, and Frederick Lanni

*Center for Light Microscope Imaging and Biotechnology
Biomedical Engineering Program, Department of Physics,
and Department of Biological Sciences
Carnegie Mellon University, Pittsburgh, Pennsylvania

ABSTRACT

Standing-wave fluorescence microscopy (SWFM), a method which utilizes interference to create a periodic excitation pattern along the optical axis, has been shown to provide improved axial resolution in thin, fluorescently labeled specimens. In each plane of focus, a complete standing wave data set is obtained by acquiring an image at each of three distinct positions of the interference fringes. Thicker specimens require through-focus data consisting of three images per plane. In this report we describe the recovery of information from this data using 3-D image processing.

The effective optical transfer function (OTF) of the standing wave microscope consists of the conventional OTF and two sidebands which are copies of the conventional OTF shifted axially by the spatial frequency of the interference fringes. The large gaps between the central band and the sidebands lead to significant ringing in the 3-D reconstruction if linear deconvolution methods are employed.

The use of non-linear, constrained image processing techniques has been shown to allow accurate extrapolation outside the OTF band limit. We demonstrate the extent to which the sidebands enhance recovery of information in the gaps, and provide a comparison between deconvolution using inverse-filtering and maximum-likelihood estimation.

1. EXPERIMENTAL APPARATUS

The analysis and simulations in this paper complement the optical system and data format of the basic standing-wave microscope in our laboratory. [1, 2] This instrument is based on a Zeiss inverted microscope (IM35), originally configured for epi-fluorescence. Specimens are mounted in an index matching medium between two coverglasses, and illuminated by counter-propagating mutually coherent laser beams of wavelength 0.5145 micron. Under these conditions, the resulting standing-wave intensity field is periodic along the optical axis, with a period of 0.1715 micron. The "phase" of the standing-wave intensity with respect to the object is controlled by changing the optical path of one of the illumination beams. Images are acquired through one of the objectives at 590 nm with additional magnification of 3.2x onto a Photometrics 512 x 512 cooled CCD camera with 19 micron square elements. The effective transverse sampling in object space is therefore 0.060 micron/pixel. Three-dimensional data sets are obtained by stepping through focus in increments of 0.25 micron and collecting three images: q, r and s, per focal plane at three phases of standing-wave illumination. The phase of the standing wave is held stationary with respect to the specimen for each q, r and s image set respectively. The relative phase between the q and r sets and between the r and s sets is $\pi/2$ radians. The phase of the standing-wave with respect to the in-focus plane of the microscope is not measured.

2. THEORY OF STANDING-WAVE FLUORESCENCE MICROSCOPY

In the standing-wave microscope, axial modulation of the illumination acts as a spatial weighting factor on the object $o(\mathbf{r})$. The modulated object is convolved with the point spread function (PSF), $p(\mathbf{r})$, of a conventional fluorescence microscope to form the image:

$$i(\mathbf{r}, \phi) = \{o(\mathbf{r})\,[1 + \cos(Kz + \phi)]\} * p(\mathbf{r}), \tag{1}$$

where ϕ is the (unknown) phase of the standing-wave illumination and * denotes convolution.

When the Fourier transform of Eq. 1 is taken,

0-8194-2029-8/96/$6.00

$$I(\mathbf{k},\phi) = P(\mathbf{k})\{O(\mathbf{k}) + \frac{1}{2}[e^{i\phi}O(\mathbf{k}+\mathbf{K}) + e^{-i\phi}O(\mathbf{k}-\mathbf{K})]\} \quad (2)$$

it is seen that a standing-wave data set contains the same Fourier components present in the conventional fluorescence image, as well as additional, higher frequency components which have been shifted by $\pm\mathbf{K} = \pm\hat{\mathbf{k}}_z K$ into the passband of the optical transfer function $P(\mathbf{k})$ (Fig. 1). By acquiring 3-dimensional data sets at three distinct phases, Eq. 2 can be solved for the central, the down-shifted and up-shifted Fourier components. It is important to point out that in the present instrument, the phase of the standing-wave with respect to the exact in-focus plane of the microscope is not measured. Therefore, the down-shifted and up-shifted Fourier components are only determined up to an overall, unknown phase factor $e^{\pm i\phi}$. As will be demonstrated, the absence of knowledge of the absolute phase complicates the object estimation process.

Three 3-dimensional image sets q, r and s are acquired at phases ϕ, $\phi + \pi/2$ and $\phi + \pi$ radians respectively. After Fourier transformation, the resulting images

$$Q(\mathbf{k}) = P(\mathbf{k})\{O(\mathbf{k}) + \frac{1}{2}[e^{i\phi}O(\mathbf{k}+\mathbf{K}) + e^{-i\phi}O(\mathbf{k}-\mathbf{K})]\} \quad (3)$$

$$R(\mathbf{k}) = P(\mathbf{k})\{O(\mathbf{k}) + \frac{1}{2}[ie^{i\phi}O(\mathbf{k}+\mathbf{K}) - ie^{-i\phi}O(\mathbf{k}-\mathbf{K})]\} \quad (4)$$

$$S(\mathbf{k}) = P(\mathbf{k})\{O(\mathbf{k}) - \frac{1}{2}[e^{i\phi}O(\mathbf{k}+\mathbf{K}) + e^{-i\phi}O(\mathbf{k}-\mathbf{K})]\} \quad (5)$$

are solved algebraically for the central, down-shifted and up-shifted Fourier components:

$$P(\mathbf{k})O(\mathbf{k}) = \frac{1}{2}[Q(\mathbf{k}) + S(\mathbf{k})] \quad (6)$$

$$\frac{1}{2}[P(\mathbf{k})e^{i\phi}O(\mathbf{k}+\mathbf{K})] = \frac{1}{4}[(1+i)Q(\mathbf{k}) - 2iR(\mathbf{k}) + (-1+i)S(\mathbf{k})] \quad (7)$$

$$\frac{1}{2}[P(\mathbf{k})e^{-i\phi}O(\mathbf{k}-\mathbf{K})] = \frac{1}{4}[(1-i)Q(\mathbf{k}) + 2iR(\mathbf{k}) - (1+i)S(\mathbf{k})]\,. \quad (8)$$

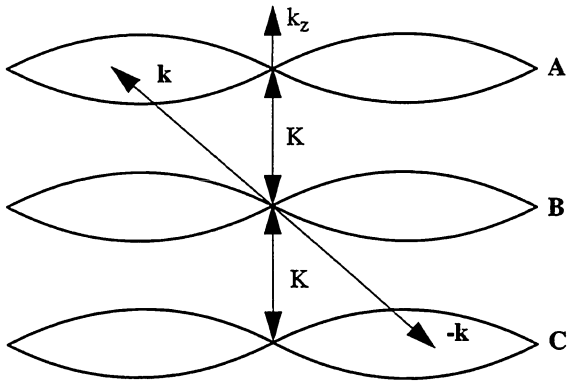

Fig. 1 The effective OTF bandpass for standing-wave fluorescence microscopy. Regions A, B, and C are shown as two-dimensional sections of the OTF band limit. The microscope objective only passes Fourier components that lie within region B. Standing-wave illumination shifts Fourier components in regions A and C into region B where they are passed by the optics. Since the object, $o(\mathbf{r})$, is a real quantity which represents the volume concentration of fluorescent dye molecules, its transform $O(\mathbf{k})$ must obey the identity $O(-\mathbf{k}) = O(\mathbf{k})^*$. The offset is $|\mathbf{K}| = 4\pi n/\lambda$ where n is the index of refraction of the specimen and λ is the excitation wavelength.

Referring to Fig. 1, it is evident that the Fourier coefficients of Eqs. 7 and 8 originate in regions A and C respectively, and have been shifted into region B by standing-wave illumination. The Fourier coefficients of Eq. 6 are equivalent to those of conventional fluorescence microscopy (FM) and belong where they are, that is, in region B. Since regions A, B and C do not overlap, a composite standing-wave data set can be constructed by applying the coordinate transformations $\mathbf{k} \rightarrow \mathbf{k} - \mathbf{K}$ and $\mathbf{k} \rightarrow \mathbf{k} + \mathbf{K}$ to Eqs. 7 and 8 and summing the result with Eq. 6:

$$I_{comp}(\mathbf{k}) = \frac{1}{2}[Q(\mathbf{k}) + S(\mathbf{k})] + \frac{1}{4}[(1+i)Q(\mathbf{k}-\mathbf{K}) - 2iR(\mathbf{k}-\mathbf{K}) + (-1+i)S(\mathbf{k}-\mathbf{K})]$$

$$+ \frac{1}{4}[(1-i)Q(\mathbf{k}+\mathbf{K}) + 2iR(\mathbf{k}+\mathbf{K}) - (1+i)S(\mathbf{k}+\mathbf{K})] \tag{9}$$

or

$$I_{comp}(\mathbf{k}, \phi) = O(\mathbf{k})\{P(\mathbf{k}) + \frac{1}{2}[e^{i\phi}P(\mathbf{k}+\mathbf{K}) + e^{-i\phi}P(\mathbf{k}-\mathbf{K})]\}. \tag{10}$$

We define (Fig. 2) the standing-wave optical transfer function (swOTF):

$$\text{swOTF}(\mathbf{k}) \equiv \{P(\mathbf{k}) + \frac{1}{2}[P(\mathbf{k}+\mathbf{K}) + P(\mathbf{k}-\mathbf{K})]\}, \tag{11}$$

and the corresponding standing-wave point spread function (swPSF):

$$\text{swPSF}(\mathbf{r}) \equiv p(\mathbf{r})\,[1 + \cos(Kz)]. \tag{12}$$

The composite image for the case $\phi = 0$ is then the convolution of the object with the swPSF:

$$i_{comp}(\mathbf{r}, 0) = o(\mathbf{r}) * \text{swPSF}(\mathbf{r}). \tag{13}$$

Equation 13 is the starting point for the object estimation process.

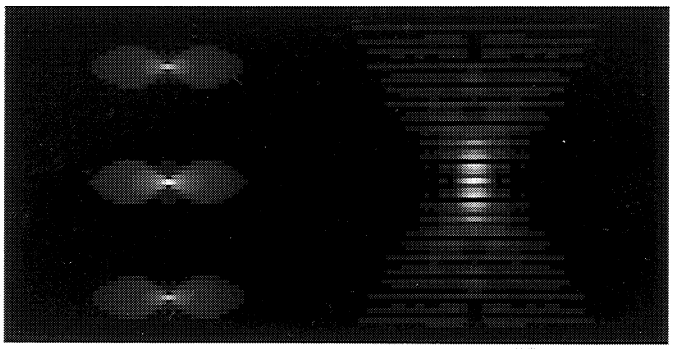

Fig. 2 A. The swOTF. The central band is identical to that of FM. The sidebands, which pass the additional information obtained by SWFM, are half the intensity of the central band and shifted by $\pm\mathbf{K}$. B. The swPSF is the product of the axially-periodic standing-wave weighting factor (1 + cos(Kz)) and the conventional PSF.

3. OBJECT ESTIMATION SIMULATIONS

As mentioned in section 2, the phase ϕ is not determined when a standing-wave data set is acquired. In addition, each successive standing-wave data set will, in principle, have a different phase offset. Equation 13 holds only for the coincidental case where the composite data set formed by Eq. 9 has $\phi = 0$. For the sake of simplicity, one-dimensional simulations were used to compare the results from linear and non-linear estimation methods and the effect of the unknown phase on the estimation process. The one-dimensional PSF was taken to be:

$$p(z) = \left[\mathrm{sinc}\left(\frac{NA^2}{2n\lambda_{em}}z\right)\right]^2 \tag{14}$$

where n is the index of refraction of the specimen and λ_{em} is the emission wavelength. The corresponding swPSF is $\mathrm{swPSF}(z) = [1+\cos(Kz)]\,p(z)$. We have verified that the results are also valid for the three-dimensional case. In sections 3.1 and 3.2 we assume that the phase is zero. Section 3.3 explores the effect of non-zero phase on object reconstruction.

3.1 Inverse filtering

Many techniques can be used to obtain an estimate of the object from Eq. 13. In the simplest method, inverse filtering, the Fourier transform (FT) of composite image, $I_{comp}(\mathbf{k})$ is divided by the swOTF, then transformed back using only values of $\mathbf{k}$ within the bandpass $\Omega(\mathbf{k})$:

$$o(\mathbf{r})_{estimate} = (FT)^{-1}_{\{\Omega\}}\left[\frac{I_{comp}(\mathbf{k})\,\Omega(\mathbf{k})}{\mathrm{swOTF}(\mathbf{k})}\right] \tag{15}$$

This method constitutes an ill-posed problem for all but noiseless simulated data, but has the advantage that the output can be calculated in closed form for simple cases. Figure 3 shows the simulated response of the inverse-filtered results of FM and SWFM when the object is an impulse and the PSF is a purely axial one-dimensional function (Eq. 14). We assume in the model that phase ϕ is known to be zero. The oscillations present in the SWFM result are due to the gaps in the swOTF band-pass (Fig. 1). Unless there is *a priori* knowledge that the axial extent of the object is less than one half standing-wave node spacing, linear methods like inverse filtering will, in general, not produce higher resolution estimates from SWFM than can be achieved with standard FM.

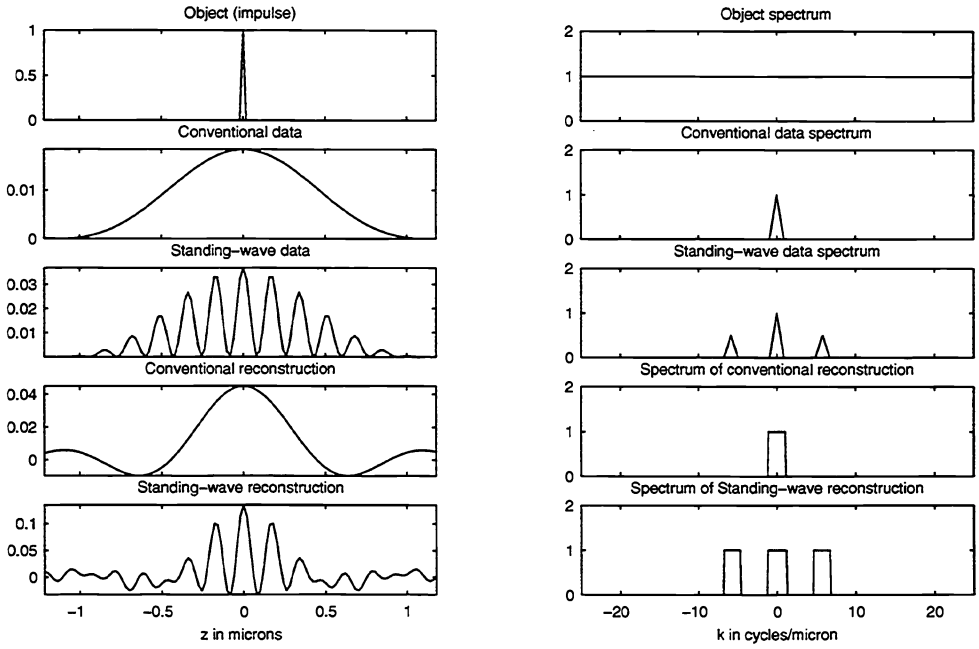

Fig. 3 The 1-D simulated, normalized result of inverse filtering in SWFM and FM. The object was taken to be an impulse at the origin and the standing wave phase ϕ was assumed to be known and equal to zero. The SWFM inverse-filtered result in this case has the FM inverse-filtered result as its envelope and is modulated by the factor $[1+2\cos(Kz)]$. Without *a priori* knowledge that the object's axial extent is less than one half the standing-wave node spacing, linear reconstructions of SWFM data are in general no better than reconstructions from FM data.

3.2 Maximum likelihood estimation

Non-linear image-processing techniques, when combined with additional constraints, have been shown to allow estimation of object Fourier coefficients beyond the band limit of a system's transfer function. In this section, maximum likelihood estimation with the added constraint that the estimate must be non-negative, was used to process simulated one-dimensional SWFM and FM data. The object was taken to be two impulses, separated by 0.080 micron. We used an iterative technique, the expectation-maximization algorithm [3, 4, 5], to obtain the maximum likelihood estimate of the object $o(\mathbf{r})$ given the image, $i(\mathbf{r})$ and the PSF, $p(\mathbf{r})$. The same algorithm, shown here in its form for the FM case:

$$o(\mathbf{r})_{n+1} = o(\mathbf{r})_n \left[\left(\frac{i(\mathbf{r})}{o(\mathbf{r})_n * p(\mathbf{r})} \right) * p(-\mathbf{r}) \right] \tag{16}$$

was also used for the SWFM simulations:

$$o(\mathbf{r})_{n+1} = o(\mathbf{r})_n \left[\left(\frac{i_{comp}(\mathbf{r})}{o(\mathbf{r})_n * swPSF(\mathbf{r})} \right) * swPSF(-\mathbf{r}) \right]. \tag{17}$$

The non-negativity constraint is automatically enforced provided the initial estimate $o(\mathbf{r})_0$ is non-negative.

Figure 4 illustrates the difference in object reconstructions for FM and SWFM simulations when the phase ϕ is known. The maximum likelihood method, implemented using the expectation-maximization algorithm, allows for extrapolation beyond the system band limit for both the FM and SWFM cases. However, only when additional information from the swOTF sidebands is included does the algorithm correctly reconstruct the two impulses.

3.3 The effect of standing-wave phase on the estimation process

The results of the previous section hold only if the phase ϕ of the composite image is zero. To illustrate this problem, we took the object to be a single impulse at the origin and formed a series of composite standing-wave images from Eq. 10 with phases from 0 to 2π radians. The expectation-maximization algorithm (Eq. 17) was run for 400 iterations for each composite image. As can clearly be seen from Fig. 5, the only satisfactory reconstruction occurs for $\phi = 0$. In a real data set collected with the standing-wave microscope, any of these reconstructions are possible for a point source object because of the unknown phase.

4. CONCLUSION

From the detailed discussion of SWFM it was shown that the composite standing-wave image is the convolution of the object with the swPSF when the phase is equal to zero. Object estimation techniques using linear methods, such as inverse filtering, were found to produce unsatisfactory outputs for SWFM. Maximum-likelihood estimation, a non-linear method, implemented via the expectation-maximization algorithm, resolved, in a one-dimensional simulation, two impulses separated axially by 0.080 micron in the case of SWFM if the phase was known. The spectrum of the reconstruction indicates that the presence of information in the sidebands significantly aids in the recovery of information in the band gaps.

The actual instrument produces composite images of unknown phase. Object estimates from these composite images are only correct for the coincidental case of $\phi = 0$. The phase of composite images can be offset by a simple manipulation [6] and an ensemble of composite images of varying phase can be generated. Each member of the ensemble will result in a different object estimate. If there is *a priori* knowledge about some feature in the object, it may be possible to reject spurious estimates and thus determine the best estimate of the object and the unknown phase.

5. ACKNOWLEDGMENTS

This research is supported by grants from the National Science Foundation (MCB-8920118, BIR-9217217, BIR-9256343), and through a grant from Carl Zeiss GmbH.

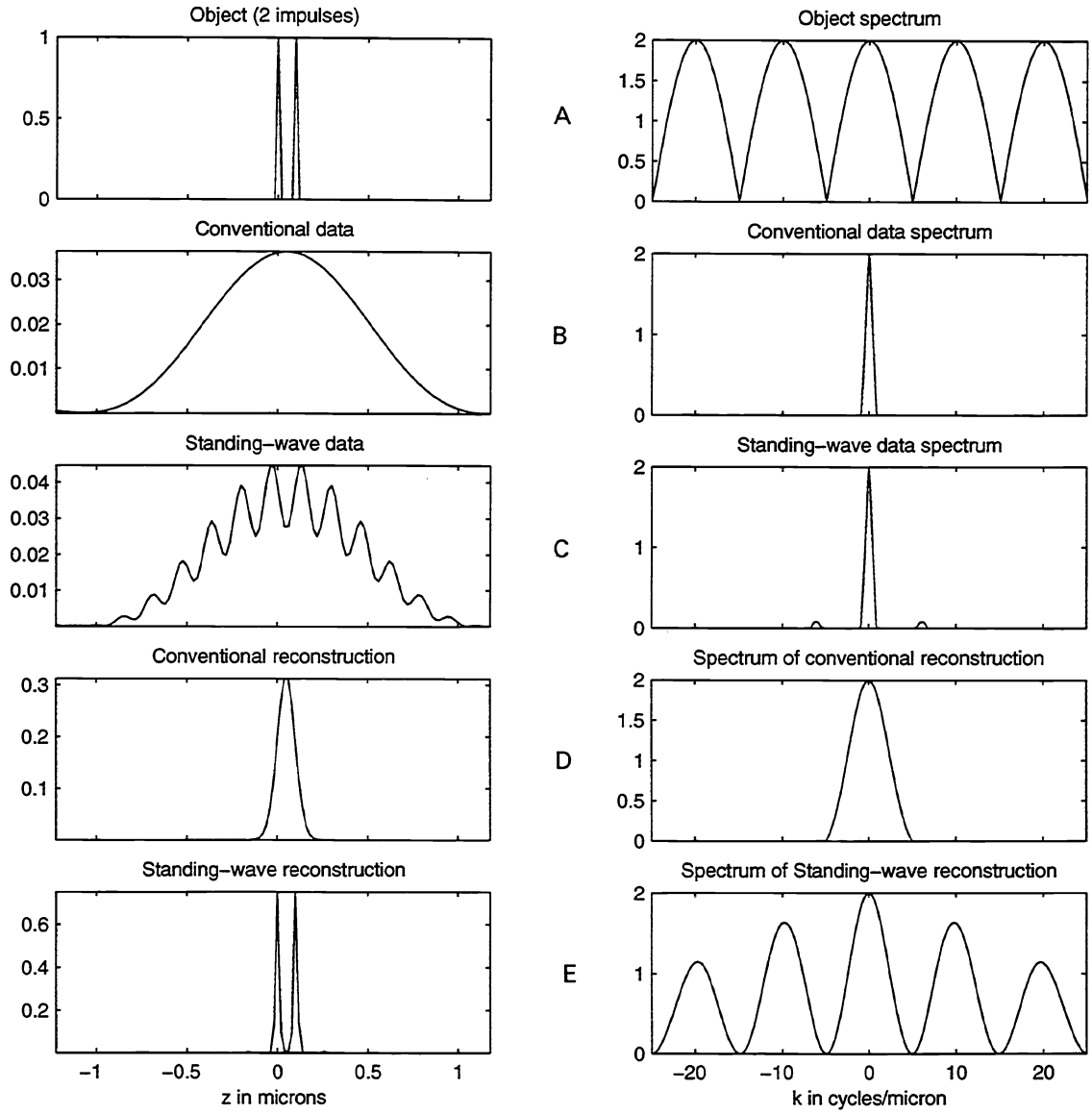

Fig. 4 One-dimensional simulations comparing SWFM and FM object estimations using the expectation-maximization algorithm. Each graph in the right column is the magnitude of the Fourier transform of the corresponding graph in the left hand column. A. The object consisted of two impulses separated by 0.080 micron. B. The (one-dimensional) image formed by convolving the object with the FM PSF. C. The composite image formed by convolving the object with the swPSF. The sidebands are weak because they happen to fall near zeroes in the object spectrum. D. The FM object estimate failed to resolve the two impulses after 1000 iterations. E. The SWFM object estimate after 1000 iterations correctly resolved the two impulses, and its spectrum closely matched that of the actual object.

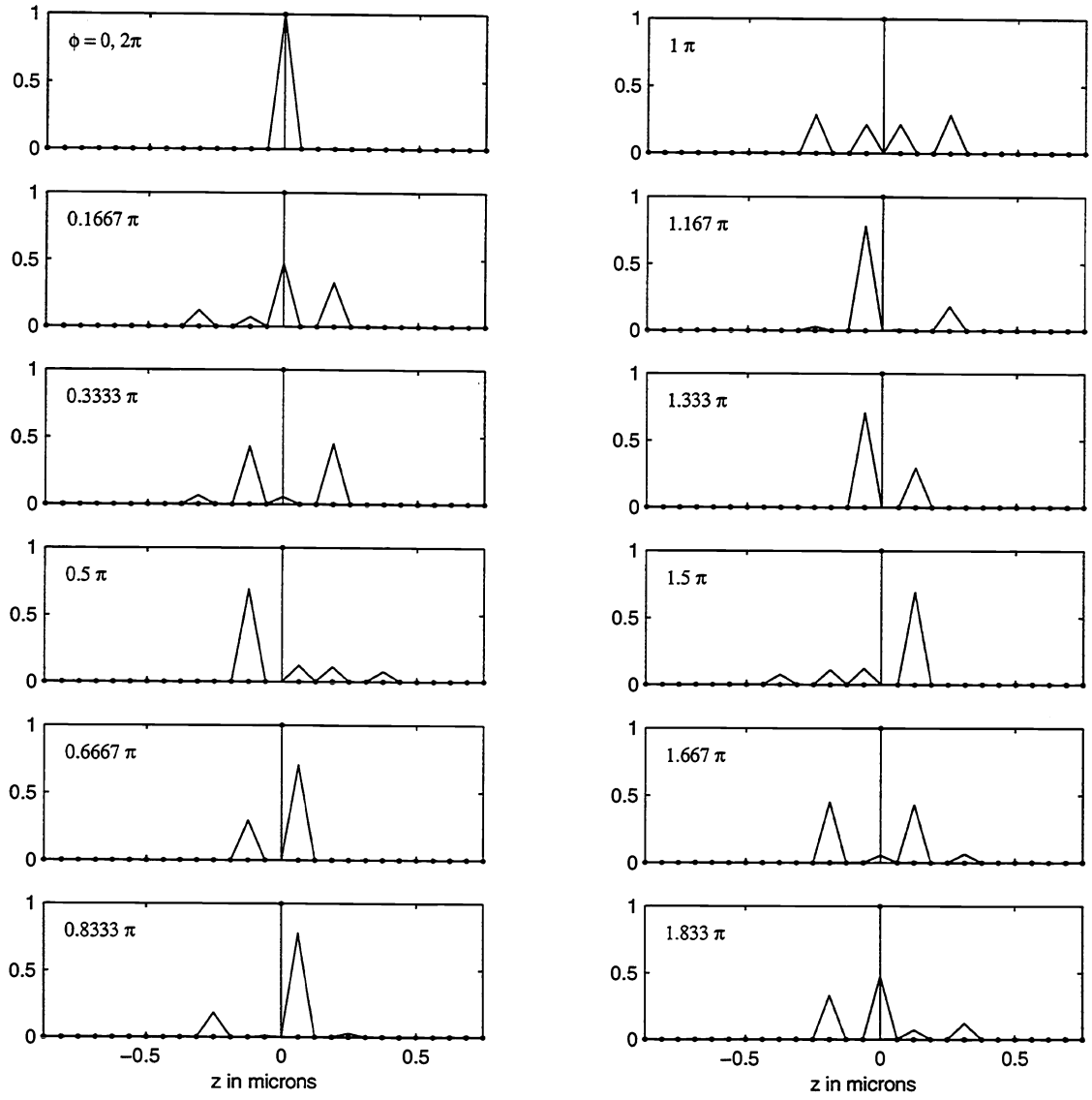

Fig. 5 The effect of phase error on the estimation process. The 1-D object was taken to be an impulse at the origin. A series of composite standing-wave "images" were created with phases ranging from 0 to 2π radians. The expectation-maximization algorithm (Eq. 17) was run for 400 iterations for each composite data set. The maximum-likelihood estimates were all stable and conserved total "photo counts" independently of the number of iterations run. However, the estimation process reconstructed the correct object only for the correct phase ($\phi = 0$).

6. REFERENCES

1. B. Bailey, D. L. Farkas, D. L. Taylor and F. Lanni, "Enhancement of axial resolution in fluorescence microscopy by standing-wave excitation," Nature, Vol. 366, pp. 44-48, 1993.

2. F. Lanni, B. Bailey, D. L. Farkas, and D. L. Taylor, "Excitation field synthesis as a means for obtaining enhanced axial resolution in fluorescence microscopes," Bioimaging, Vol. 1, pp. 187-196, 1993.

3. A. P. Dempster, N. M. Laird, and D. B. Rubin, "Maximum likelihood from incomplete data via the EM algorithm," J. Roy. Stat. Soc. B 39, pp. 1-37, 1977.

4. L. A. Shepp and Y. Vardi, "Maximum likelihood reconstruction for emission tomography," IEEE Trans. Med. Imag., MI-1, pp. 113-121, 1982.

5. T. J. Holmes, "Maximum-likelihood image restoration adapted for noncoherent optical imaging," J. Opt. Soc. Am. A, Vol. 5, pp. 666-673, 1988.

6. B. Bailey, V. Krishnamurthi, D. L. Farkas, D. L. Taylor, F. Lanni, "Three-dimensional imaging of biological specimens with standing-wave fluorescence microscopy," *Proc. Soc. Photo-optical Instr. Eng.* 2184, pp. 208-213, 1994.